# CALCULATION OF THE NON LINEAR AERODYNAMIC COEFFICIENTS OF WINGS OF VARIOUS SHAPES AND THEIR WAKES, INCLUDING CANARD CONFIGURATIONS.†

J. Rom*, D. Almosnino** and C. Zorea***
Technion, Israel Institute of Technology

## Abstract

This paper introduces a method for the calculation of the non linear, longitudinal aerodynamic characteristics of various planar shapes, including multiple lifting surface configurations in subsonic flow, at high angles of attack.

The method developed can handle complex planforms such as closely coupled canard-wing combinations, wing-tail combinations, cruciform types of wing arrangements, various flaps, elevators, dihedral angles as well as ground effect problems.

The present work uses a modified "Vortex Lattice Method", by including the effects of the shedding and of the development of the rolled-up wake.

The solution is carried out by an iterative process, saving a lot of computing time.

Comparisons with experimental data show very good agreement even in cases of very strong non linear effects of leading edge vortices, or in cases of side-edge vortices rolling up above the surface of low aspect ratio wings.

This method results in the evaluation of the shape and strength of the secondary vortex which had already been observed in experiments, and local pressure effects caused by vortices passing over a wing surface in the multiple lifting surface configurations.

## List of Symbols

| | |
|---|---|
| AR | aspect ratio, $b^2/S$ |
| b | wing span |
| C | chord |
| $C_{D_i}$ | induced drag coefficient $D_i/qS$ |
| $C_{D_o}$ | parasite drag coefficient $D_o/qS$ |
| $C_L$ | lift coefficient, L/qS |
| $C_\ell$ | section lift coefficient |
| $C_M$ | pitching moment coefficient M/qS $C_{Ref.}$ |
| $D_i$ | induced drag force |
| $D_o$ | parasite drag force |
| H | geometric influence matrix |
| i | index |
| j | index |
| K | strength of a vortex segment |
| L | lift force |
| M | pitching moment |
| $N_c$ | number of sub-divisions, chordwise |
| $N_s$ | number os sub-divisions, spanwise |
| q | dynamic pressure, $1/2\ \rho V^2$ |
| r | distance from a point to a vortex segment |
| S | wing area |
| U | free stream velocity |
| u,v,w | velocity distrubances in x,y,z directions accordingly |
| $\hat{w}$ | component of free stream velocity normal to a surface |
| x,y,z | Cartesian coordinates |
| $x_{c.p.}$ | center of pressure-position |
| $\alpha$ | angle of attack |
| $\rho$ | air density |

## I. Introduction

One of the most complicated and interesting problems of aerodynamicists today is the design of complex lifting surface configurations and the calculation of their aerodynamic characteristics in subsonic flow and at high angles of attack.

One of the more demanding problems is the calculation of the influence of mutual interaction between closely coupled lifting surfaces.

The formation of strong vortices over low aspect ratio wings has been recognized as beneficial for aircraft performance (Concorde, Mirage IIIc etc.). The interaction between the vortex flow field of a closely coupled canard configuration is used in the Viggen and in the Kfir C-2 airplanes. Vortex interaction effects are also obtained due to leading edge "saw-tooth" addition as well as by strakes placed at the nose of the configuration.

There are a number of methods for the calculation of aerodynamic characteristics of wings presented by Maskew [1,2], Margason and Lamar[3], Woodward[4] as well as the Boeing method [5,6].

Maskew's method [1,2] includes the effect of the rolling up of the wake, but is unable to model the leading edge vortices and the non linear lift generated due to their effects. Margason and Lamar[3] or Woodward's programs[4] do not take into account the rolling up of the wake, and therefore cannot

†This research was supported in part by the Air Force Office of Scientific Research (AFSC), United States Air Force, under Grant AFOSR 71-2145. From October 1977 the research program on non linear aerodynamic characteristics at high angles of attack is supported in part by the U.S. Army under Grant DAERO-78-G-021.

* Professor, Lady Davis Chair in Experimental Aerodynamics

** Graduate Student, Instructor

*** Adjunct Lecturer

evaluate the aerodynamic characteristics at high angles of attack.

Modifications of the last two methods try to evaluate the non linear lift by super imposing Polhamus[7] and modified Polhamus[8] methods on the linear results. However, in these cases the results are not always accurate and do not model the flow field, the local effects, the correct load distribution or effects of interactions.

The method developed by Rubbert[5,6] et al. using a doublet lattice resulted in a much refined program, and its results are accurate in many cases.

The method takes into account the rolling up of the wake and its effect on the wing. However, the use of Smith's[9] model of conical flow to describe the initial form of the leading edge vortices results in an incomplete model which cannot deal with secondary separation, or with closely interacting lifting surfaces.

The present work tries to handle wings and their wakes as one system, using the concepts of a modified vortex lattice method developed by Rom and Zorea[10,11,12,13] and by Rom, Zorea and Almosnino[14].

In the present investigation a generalized method is developed which is capable of dealing with the rolled up wake and with leading edge vortices existing in various aerodynamic planar shapes, enabling the analysis of their aerodynamic characteristics at high angles of attack.

## II. Basic Concepts

The lifting surfaces of the configuration, (such as wing, canard, horizontal tail, etc.), are divided into sub-surfaces (Fig. 1). Each subsurface is then divided into trapezoidal or triangular cells. A bound "horse-shoe" vortex is placed in each cell, as described in Fig. 1. In order to satisfy the boundary condition for the flow to be parallel to the surface of the wing, a control point is placed in each cell. (Fig. 1). The shedding of the free vortices (which represent the wake) is presented as an option for the user, who has a large variety of possibilities available (for example: from trailing edge, side edges, leading edge). Each free vortex is divided into a number of finite segments, and a half-infinite last segment. The Biot-Savart law enables the calculation of the velocity induced by a vortex segment $\overline{AB}$ of strength $K$ on a point $C$ in the flow field:

$$V_c = \frac{K \cdot (\cos \hat{BAC} + \cos \hat{CBA})}{4\pi r} \qquad (1)$$

(The last equation is in scalar form, and "r" is the distance between the point C and the segment AB).

The iterative procedure starts with the calculation of a geometric influence matrix, with the free vortices being straight lines shed at an angle to the surface, as an initial condition.

The boundary condition at the control points enables the construction of a set of linear equations. A typical form is:

$$\left[\begin{array}{c|c|c} H_{11} & H_{12} & H_{13} \\ (nxn) & (nxm) & (nxk) \\ \hline H_{21} & H_{22} & H_{23} \\ (mxn) & (mxm) & (mxk) \\ \hline H_{31} & H_{32} & H_{33} \\ (kxn) & (kxm) & (kxk) \end{array}\right] \cdot \left[\begin{array}{c} K_1^1 \\ \vdots \\ K_n^1 \\ \hline K_1^2 \\ \vdots \\ K_m^2 \\ \hline K_1^3 \\ \vdots \\ K_k^3 \end{array}\right] = \left[\begin{array}{c} \hat{w}_1^1 \\ \vdots \\ \hat{w}_n^1 \\ \hline \hat{w}_1^2 \\ \vdots \\ \hat{w}_m^2 \\ \hline \hat{w}_1^3 \\ \vdots \\ \hat{w}_k^3 \end{array}\right] \qquad (2)$$

Each sub-matrix $H_{ij}$ represents the influence of subsurface i on subsurface j. (In the example above there are three subsurfaces). The order of each submatrix is written in parenthesis, and n, m, k defines the number of cells in each of the subsurfaces 1, 2, 3 accordingly. The strength of the bound vortex in cell number j, of subsurface i is denoted by $K_j^i$, while $\hat{w}_j^i$ is the component of the free stream velocity normal to the surface of the wing, at the control point of cell number j, of subsurface i. Column vector $K_j^i$ is to be solved. When the program is solved for the strength of the bound vortices, it also calculates the aerodynamic coefficients, checking for their convergence (except for the first cycle).

The aerodynamic coefficients are $C_L$, $C_{D_i}$, $C_M$. The program also calculates the center of pressure $X_{cp}$, according to the following formulae:

The lift coefficient (including all possible terms):

$$C_L = \frac{2}{S_{Ref}} \int_o^{b/2} C_j C\ell_j dy = \frac{4}{US_{Ref.}} \sum_{j=1}^{N_s} \{ \sum_{i=1}^{N_c} [(1 + \qquad (3)$$

$$+ \frac{u}{U} - \frac{v}{U}\frac{\Delta x}{\Delta y}) \cdot K]_{ij} \Delta y_j \} + \frac{-4}{US_{Ref.}} \sum_i \sum_j (\frac{v}{u} \cdot \Delta K \cdot \Delta x)_{ij}$$

Here $\Delta X_{ij}$, $\Delta y_{ij}$, $\Delta z_{ij}$ are the cartezian components of a bound vortex segment ij in the direction x, y, z accordingly, while $u_{ij}$, $v_{ij}$, $w_{ij}$ are the disturbance velocities calculated in the middle point of each vortex segment belong to the wing surface. The second term on the right hand side of Eq. (3) is of second order, and it expresses in general form the part of the in-surface trailing vortices to the lift, being usually ignored.

The induced drag coefficient and the pitching moment coefficient are given in Eq. (4) and (5):

$$C_{D_i} = \frac{2}{S_{Ref.}} \int_o^{b/2} C_j C\ell_j \ (tg\alpha_{ind.})_j \ dy = \qquad (4)$$

$$= \frac{-4}{US_{Ref.}} \sum_{j=1}^{N_s} \sum^{N_c} [(\frac{w}{U} \Delta y + \frac{v}{U} \Delta z) \cdot K]_{ij}$$

$$C_M = \frac{4}{US_{Ref.}} \sum_{j=1}^{N_s} \{ \sum_{i=1}^{N_c} [(1 + \frac{u}{U} - \frac{v}{U}\frac{\Delta x}{\Delta y}) \cdot K]_{ij} \Delta y_j \cdot$$

$$\cdot \frac{(X_{ij} - X_{Ref.})}{C_{Ref.}} \} + \frac{-4}{US_{Ref.}} \sum_{i=1}^{N_s} \{ \sum_{i=1}^{N_c} [ \qquad (5)$$

$$[(\frac{W}{U} \Delta y + \frac{v}{U} \Delta z) \cdot K]_{ij} \frac{(Z_{ij} - Z_{Ref.})}{C_{Ref.}} \}$$

$X_{Ref.}$, $Z_{Ref.}$ are x and z coordinates of pitching moment reference point. The second term on the right-hand side of Eq. (5) expresses the rolling moment because of induced drag, and it is not negligible in the calculations of complex configurations, such as canard-wing at high angles of attack.

The center of pressure is given by definition:

$$X_{c.p.} = \frac{-C_{Ref.} \cdot C_M}{C_L} \qquad (6)$$

(measured from $X_{Ref.}$)

In general, it should be noted that some of the assumptions made when neglecting terms like those containing the effect of sidewash, proved to be incorrect in strong interactions between canard wake and wing surface, and in the case of strong leading edge vortices. Thus the calculation of aerodynamic coefficients in general cases should include all possible contributing factors.

The program uses an iterative process for the re-calculation of the trajectories of the free vortices, until convergence of aerodynamic coefficients is achieved. (The strength of those is calculated after the solution for the strength of the bound vortices).

The procedure is as follows:

Each point (i) of a segment of a free vortex is moved according to Euler's method of integration:

$$y_i^{(2)} = y_{i-1}^{(2)} + \frac{v_i^{(1)}}{U + u_i^{(1)}} \Delta X \qquad (7)$$

$$z_i^{(2)} = z_{i-1}^{(2)} + \frac{w_i^{(1)}}{U + u_j^{(1)}} \Delta X \qquad (8)$$

Here $u_i^{(1)}$, $v_i^{(1)}$, $w_i^{(1)}$ are the cartezian components of the induced velocity on point (i), before moving it. $y_i^{(2)}$, $z_i^{(2)}$ are the new y and z coordinates of point (i). (The flow is considered steady).

More sophisticated integration methods should be applied in cases where strong disturbances are expected, such as in the cases of very close interactions between lifting surfaces, or very low aspect ratios. The integration process continues iteratively until convergence of all free vortices is achieved, or until the process exceeds a prefixed number of iterations. The influence matrix is recalculated, leading to a new strength of each bound vortex. Aerodynamic coefficients are then recalculated, and all the process starts again until convergence of the coefficients is achieved.

The effect of compressibility is taken into account by applying Goethert rule and incorporating it into the computer program.

The accuracy of this rule and its application to the vortex flow over wings has been discussed also by Rubbert and Brune[20].

By using this compressibility correction, the present method can now be used over the range of subsonic Mach numbers up to the critical Mach number.

## III. Results

### General

The use of the Modified Vortex Lattice Method enabled the evaluation of the longitudinal aerodynamic characteristics of various wings as presented in Ref. 10 to 13. This method can be extended (see Ref. 14) to multiple surface configurations. These may include, for example, closely coupled canard wings, leading edge strakes and also deflected flaps on low aspect-ratio wings. All of these are characterized by the non-linear variation of the aerodynamic coefficients.

### (a) Computational Aspects

The use of the singular vortex element in vortex lattice methods presents some difficulties. The main one is the too high velocities induced by the vortex on points which are too close to the vortex segment. The reason for that is the fact that a potential singular vortex does not exist, due to viscous effects. Some attempts were made to overcome this problem, for example Rom and Zorea's[10] attempt to use the model of Spreiter and Sacks[19] for the calculation of the radius of each vortex core, or Maskew's "Sub Vortex Techniques"[1]. One of the main conclusions from these attempts was that it is satisfactory in most cases to use a general "cut off distance" for all the vortices in the model. The last method saves a lot of computing time, and it was used in the present method. The results show that it is reasonable to use a "cut off distance" similar to the width of the partition into elemental panels. Strong vortices such as those shed from a leading edge may require a larger "cut off distance".

Another problem arises when shedding too many free vortices. Because of the singularity of each potential vortex, the convergence of the free vortices trajectories is either very slow or completely impossible. The multiplicity of free vortices is a result of a dense partition into elemental panels, (which is favorable when the aim is to achieve a smoother load distribution). The present method overcomes this difficulty by giving the option to merge close free vortices into one vortex, of a strength which is the sum of the strength of the merged vortices. The number of free vortices is thus reduced, while the number of elemental panels remains as it was.

Results of the present method show that merging too close free vortices is especially effective in the cases of leading edge separation, in wings of

low aspect ratio (AR < 2) with sharp leading edges. In these cases the convergence was much more rapid and the nonlinear aerodynamic coefficients calculated showed very good agreement with experimental results. When no merging was applied, the calculated results showed weaker non linear behavior than expected, resembling experimental results for wings with round leading edges, (see for example Ref. 16). The effect of merging free vortices on aerodynamic coefficients is strong when dealing with vortices which pass upon the wing surface; Otherwise the effect is negligible.

b) Comparison with experimental results

1. Closely coupled canard and wing, with leading edge separation

The configuration was chosen for comparison with Ref. (15) and it is shown in Fig. 2. Both the canard and the main wing are of aspect-ratio 1.66, and of similar form. Two vertical positions of the canard were checked, as it is shown in Fig. 2. The canards are vertically located at $z/\bar{C}_c$=0.2, (-0.29) above (beneath) the main wing plane accordingly, and their aft point is located longitudinally at $0.1\bar{C}_c$ from the main wing vertex. (Here $C_c$ is the canard mean geometric chord). Behrbohm(15) states that the model used for the experiments had round leading edges, which considerably reduce the non linear effects. Indeed, when using the present method with the option of merging free vortices, (the effect of which was described before in part (a) of this chapter), the calculated results for the lift coefficient of the high canard were higher than the experimental ones (Fig. 3a, upper curve).

By assuming separation of vortices without merging to be a better approximation to the actual separation from the rounded leading edges, the calculated results obtained were better than those previously described, although somewhat lower than the experimental ones (Fig. 3a). The first results however, may be an indication for the maximum non linear effect that can be obtained, should the leading edges be sharp.

It should be noted that the present method also gives the correct tendencies for the low canard, in comarison with the high canard. The interesting behavior of the low canard can be observed in Fig. 3b, where the lift coefficient increases linearly up to an angle of attack of approximately 15°, and then a strong non linear effect occurs, up to 20°.

This phenomenon has been observed both in the experimental and the calculated results. It is explained by the fact that the free vortices of the canard stay below the main wing surface up to a certain point, and as the angle of attack increases above that point, the free vortices shed from the canard pass above the main wing surface, causing positive interference and as a result non linear lift is obtained. The low canard lift coefficient even equals the high canard lift coefficient at an angle of attack of 20°.

Correct tendencies for the high and low canards can be observed also from Fig. 4 where the change in the pitching moment coefficient is described (versus the lift coefficient).

The effect of interaction between high canard leading edge vortices and wing leading edge vortices can be seen from Fig. 5. Noteworthy too is the fact that due to the upwash effect of the wing on the canard, the leading edge vortices of the canard leave its surface at an angle higher than half of the angle of attack. In general, this accepted initial value which was fair enough for single wings, may lead to numerical problems in some of the strong interaction problems such as the case of a low canard. In the latter case numerical problems arise because of unfitting initial conditions, when the wake of the canard tries to cut though the wing surface. The low canard case also shows tendencies of instability in the flow, within a limited range of angles of attack. However, the high canard case which is much more common does not present any problems. An example of the load distribution is presented in Fig. 6.

2. Canard and wing interference with no leading edge separation.

The configurations chosen were three variations of a basic model experimented by Gloss(17). The basic form of the configuration is shown in Fig. 7. The model consists of a trapezoidal main wing of AR = 2.5 and a swept back canard of AR = 4.12. The first variation (denoted as configuration No. 2) consists of a 51.7 deg. swept back canard, which has 0 deg. dihedral angle. The second variation (denoted as configuration No. 3) consists of a 51.7 deg. swept back canard which has 18.6 deg. dihedral angle. The third variation (denoted as configuration No. 4) consists of a 60 deg. swept back canard which has 0 deg. dihedral angle.

All canards' roots were located at a height of $z/\bar{C}$ = 0.185 above the wing plane, ($\bar{C}$ is the wing mean geometric chord), and at a longitudinal distance of $x/\bar{C}$ = 1.304 from the model nose to the canard leading edge. The partition chosen for the calculations was NC = 4, NS = 10 (using trapezoidal cells) both for the canard and for the main wing, in all cases.

Free vortices were shed from the trailing edges and from the side edges. All three cases showed very good agreement between the experimental and the calculated results as can be seen from Figs. 8 to 12. The calculated results depart from the experimental results only when stall effects start. Trying a denser partition of NC = 4, NS = 10 for the canard, with NC = 10, NS = 20 for the main wing had very little effect on the results, apart from the higher computer time needed for the solution.

An interesting comparison is shown in Figs. 13 and 14. The present method is compared to calculated results of modified Polhamus methods (from Ref. 17). It can be seen clearly that the present results for the lift coefficient are in better comparison with the experimental results, in addition to the evaluation of the load distribution and the strength and form of the wake, which are not calculated by the modified Polhamus methods.

3. Secondary vortex formation

As an example of this phenomenon a view of main and secondary leading edge vortices was sketched for a delta wing of AR = 2, at 20 deg. angle of

attack (Fig. 15). The calculated relative strength of those vortices appear in a table (Fig. 15). (Trailing edge vortices were omitted from Fig. 15 in order to get a clearer view). In delta wings of AR < 2, the appearance of the secondary vortex is found to be at an inner region than the example given, as indicated by experiments.

4. The F-4-E planform in compressible flow.

In the following example application of the method has been made to analyse a complex planform also making use of the Goethert rule for the evaluation of the compressibility effects.

The geometry of the model includes the main wing which has a dihedral of 12 deg. on its outer span and a "saw tooth" form on its leading edge. The tail planform has a negative angle of dihedral (-23.25 deg.) and is operating as a mono-bloc control. Both the main wing and the tail are extended to the center line. A schematic description of the geometry of the model, partitioned into elemental panels is shown in Fig. 16. The calculated results are compared with the experimental results of Ref. 18. Very accurate results are obtained for the lift coefficient variation with the angle of attack, at M = 0.6 and also at M = 0.8, up to the stall conditions, (Fig. 17).

Good results are also obtained for tail deflections up to -16 deg. There was no point in comparing results for the pitching moment, because of the difficulty to correct the calculations for the presence of the complex body; however, deflections of the tail show the right tendencies in the calculated pitching moment.

The experimental results for induced drag coefficient fall between the calculated results for the case of full leading-edge suction drag and those calculated for zero leading-edge suction drag, (Fig. 18). (See also a note about calculation of the induced drag in part (d) of this chapter).

c) Cruciform configuration in subsonic flow

The non linear characteristics of a cruciform combination of rectangular wings are evaluated by the present method (at 0.0 Mach number). The configuration is combined of cruciformed rectangular main wings and tails, described in Fig. 19. The calculated lift and pitching moment coefficients show a strong non linear variation with increasing angle of attack (Fig. 20). The existence of the "turning point" in the curves of $C_L$, $C_M$, $C_{D_i}$ (Fig. 20) is explained by examining the path of the free vortices shed by the wing. At about 12° those vortices pass very near and below the upper tail, causing a considerable loss of lift on that part. Further increase of the angle of attack would cause those free vortices to make their way above tail, gaining lift again. It should be noted that there is some loss of stability in the region of the turning point, as seen from the pitching moment curve slope. Experimental data on cruciformed wings configurations indicate similar variation. Results are sensitive to the relative location and shape of the tail.

d) A note on the calculation of induced drag

Vortex lattice methods (including the present work) tend to give a low value for the induced drag coefficient, calculated by Eq. (4). It seems that the reason for this fact is due to the method itself. One aspect of the problem is caused by the somehow incorrect induced velocities calculated by the method near the leading edge. Another aspect is due to the fact that vortex lattice methods assume full leading edge suction, such as is obtained from thick wings with round leading edges. When applying the method to wings with sharp leading edges, where there is almost zero leading edge suction, the present method consistently gives a low value for $C_{D_i}$. However, in the latter case it seems that using the simple formula

$$C_{D_i} = C_L \times tg\alpha \qquad (9)$$

gives very accurate results. Nevertheless, the problem of calculating the induced drag needs further investigation, directed to include the effect of thickness.

e) Computer time

Computing time for a complex configuration is at present rather high (about 2000 sec. on IBM 370/168 type). However, computation time may be considerably reduced, should the program be optimized. The use of the iterative scheme is time saving in itself.

## IV. Conclusions

The present method offers an efficient means of analysis and design of complex aerodynamic configurations. The good results obtained for strong interaction cases and non linear effects encourage future development and refinement of the method to enable the analysis of configurations which may also include body and thickness effects. Aerodynamic characteristics at high angles of attack can be successfully analysed using this method up to the effects of stall or vortex breakdown.

## V. References


1. "Vortex Lattice Utilization," Workshop held at NASA Langley R.C., NASA SP-405, May 1976.

2. Maskew, B., "Calculation of the three-dimensional potential flow around lifting non planar wings and wing-bodies using a surface distribution of quadrilateral vortex rings," Loughborough U. of Tech., Rep. TT 7009, Sept. 1970.

3. Margason, R.J. and Lamar, J.E., "Vortex Lattice FORTRAN program for estimating subsonic aerodynamic characteristics of complex planforms," NASA TN D 6142, Feb. 1971.

4. Woodward, F.A., "An improved method for the aerodynamic analysis of wing-body-tail configurations in subsonic and supersonic flow," NASA CR-2228 (2 volumes), May 1973.

5. Rubbert, P.E. and Saaris, G.R. "Review and Evaluation of a three-dimensional lifting potential flow analysis method for arbitrary configurations," AIAA Paper 72-188, Jan. 1972.

6. Weber, J.A., Brune, G.W., Johnson, F.T., Lu, P. and Rubbert, P.E. "A three-dimensional solution of flows over wings with leading edge vortex separation," NASA SP-347, 1975, pp. 1013-1032. Also, AIAA Journal, Vol. 14, No. 4, April 1976,

pp. 519-525.

7. Polhamus, E.G., "A concept of the vortex lift of sharp edge delta wings based on a leading edge suction analogy," NASA TND-3767, Dec. 1966.

8. Lamar, J.E., "Some recent applications of the suction analogy to vortex lift estimates," NASA SP-347, pp. 985-1011, 1975.

9. Smith, J.H.B., "A theory of the separated flow from the curved leading edge of a slender wing" Tech, Note Aero 2535, Nov. 1957.

10. Rom, J., Zorea, C., and R. Gordon, "On the calculation of nonlinear aerodynamic characteristics and the near vortex wake," ICAS Paper No. 74-27, Aug. 25-30, 1974.

11. Rom, J., Portnoy, H., and Zorea, C., "Investigations of the rolling-up of the vortex wake and calculation of non linear aerodynamic characteristics of wings," TAE Rep. No. 277, Technion, Israel Institute of Technology, June 1976.

12. Zorea, C. and Rom, J., "Vortex rollup over and behind wings related to non linear aerodynamic characteristics," Journal of Aircraft, Vol. 15, No. 4, April 1978, pp. 193-194.

13. Zorea, C.R. and Rom, J., "The calculation of non-linear aerodynamic characteristics of wings and their wakes in subsonic flow," Proceedings of 20th Israel Annual Conference on Aviation and Astronautics, February 1978, pp. 36-48.

14. Almosnino, D., Zorea, C. and Rom, J., "A method for calculating longitudinal characteristics of wings and multiple lifting surfaces in subsonic flow, and at high angles of attack," Proceedings of 20th Israel Annual Conference on Aviation and Astronautics, February 1978, pp. 66-74.

15. Behrbohm, H., "Basic low speed aerodynamics of the short coupled canard configuration of small aspect ratio," SAAB TN-60, Sweden, July 1965.

16. Kuchemann, D., "A nonlinear lifting-surface theory for wings of small aspect ratio with edge separation," Royal Aircraft Estab. Rep. AERO 2540, April 1955.

17. Gloss, B.B., "The effect of canard leading-edge sweep and dihedral angle on the longitudinal and lateral aerodynamic characteristics of a close coupled canard-wing configuration," NASA TND-7814, Dec. 1974.

18. Ray, E.J. and Hollingsworth, E.G., "Subsonic Characteristics of a twin jet swept-wing fighter model with maneuvering devices," NASA TN D-6921, Jan. 1973.

19. Spreiter, J.R. and Sacks, A.H., "The rolling up of the trailing vortex sheet and its effects on the downwash behind the wings," J.A.S. Vol. 18, No. 1, Jan. 1951, pp. 21-32.

20. Brune, G.W. and Rubbert, P.E., "Boundary-value Problem of configurations with compressible free vortex flow," AIAA Journal Vol. 15, No. 10, pp. 1521-1523, October 1977.

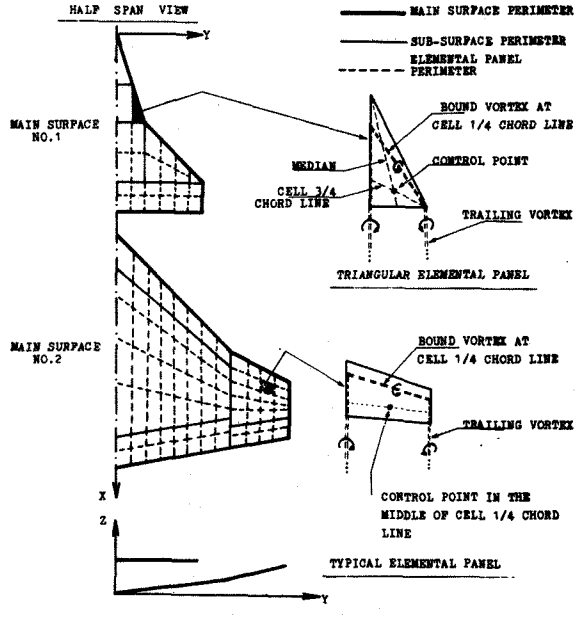


FIGURE 1 - DESCRIPTION OF THE MODEL.

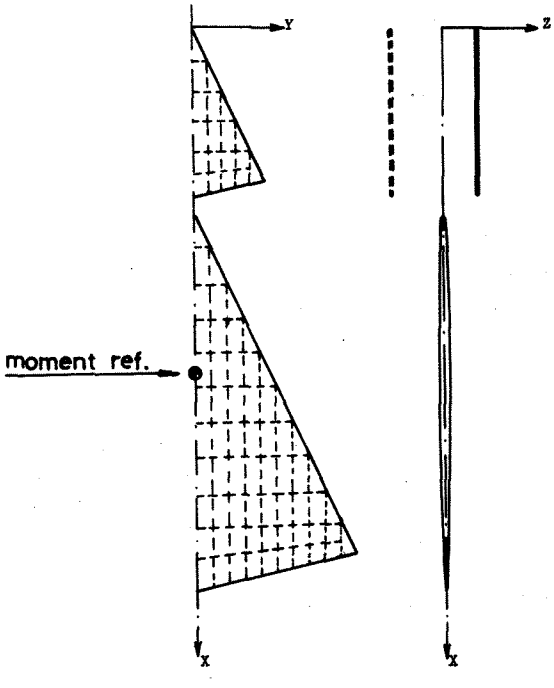


FIGURE 2 - COMPARISON WITH EXPERIMENTAL RESULTS - REF. 15; *CANARD CONFIGURATION NO. 1 PARTITIONED INTO* ELEMENTAL PANELS.

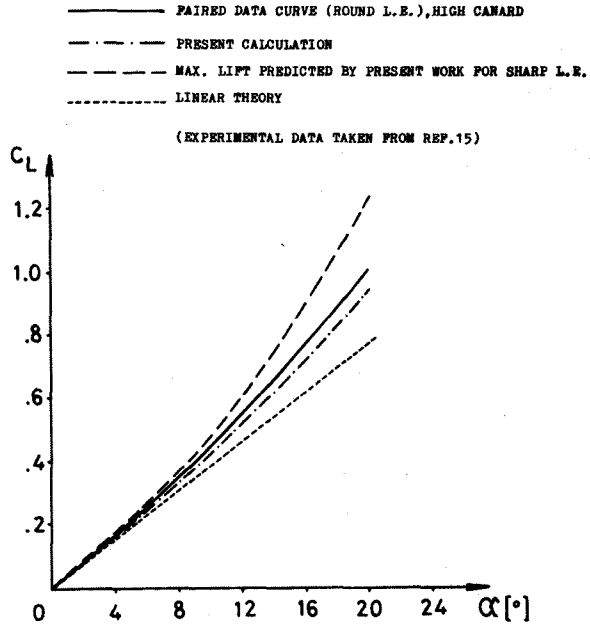


FIGURE 3-a - LIFT COEFFICIENT Vs. ANGLE OF ATTACK FOR CONFIGURATION No. 1, HIGH CANARD.

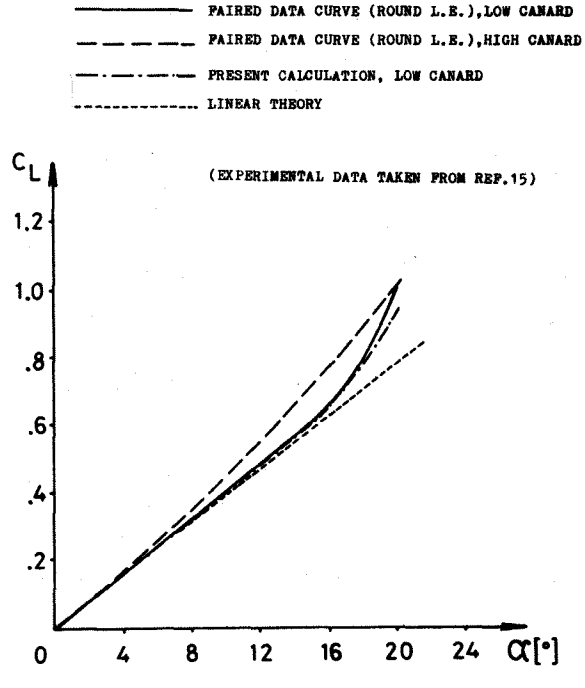


FIGURE 3-b - LIFT COEFFICIENT Vs. ANGLE OF ATTACK FOR CONFIGURATION No. 1, LOW CANARD.

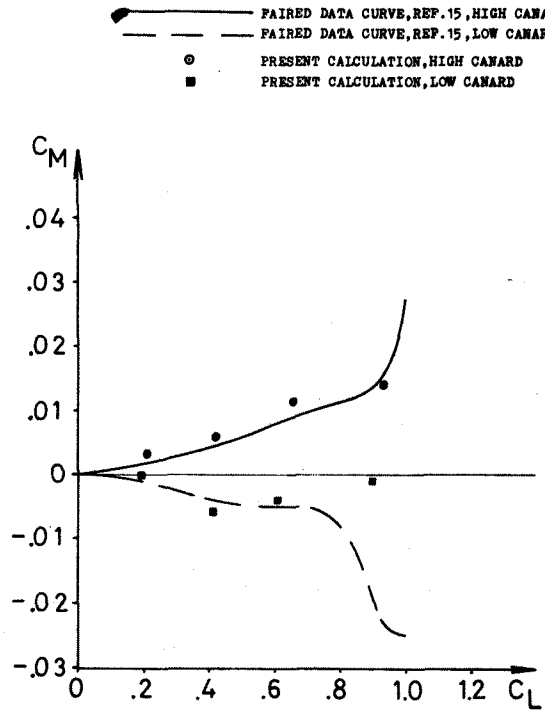


FIGURE 4 - PITCHING MOMENT COEFFICIENT Vs. LIFT COEFFICIENT FOR HIGH AND LOW CANARDS, CONFIGURATION No. 1.

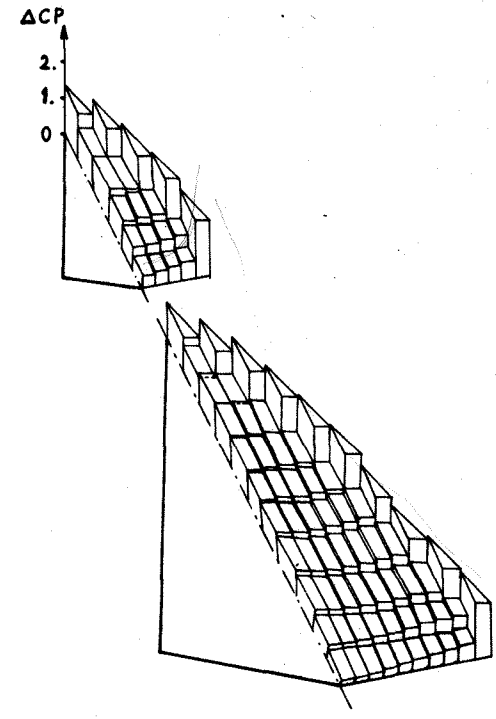


FIGURE 5 - AN EXAMPLE OF CALCULATED LOAD DISTRIBUTION OF WING AND CANARD AT 20 DEG. ANGLE OF ATTACK, CONFIGURATION NO. 1.

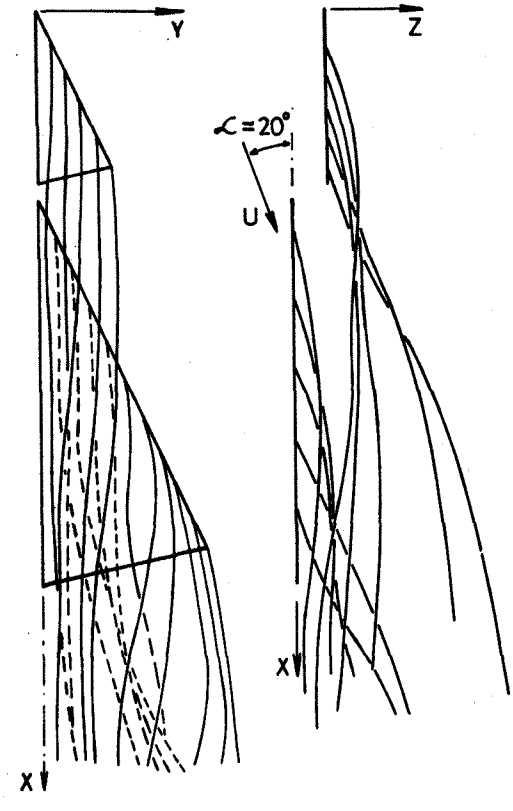


FIGURE 6 - CALCULATED INTERACTION BETWEEN CANARD AND WING LEADING EDGE VORTICES, CONFIGURATION NO. 1.

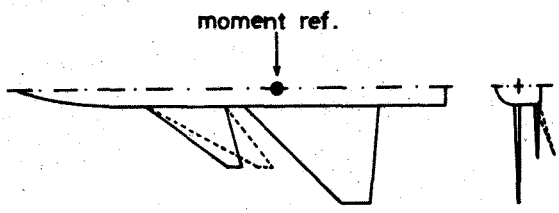


CONFIG. NO.2 : 51.7° CANARD L.E. SWEEP, 0° DIHEDRAL
CONFIG. NO.3 : 51.7° CANARD L.E. SWEEP, 18.6° DIHEDRAL
CONFIG. NO.4 : 60° CANARD L.E. SWEEP, 0° DIHEDRAL

FIGURE 7 - COMPARISON WITH EXPERIMENTAL RESULTS - REF. 17, WING CANARD CONFIGURATIONS Nos. 2, 3, 4.

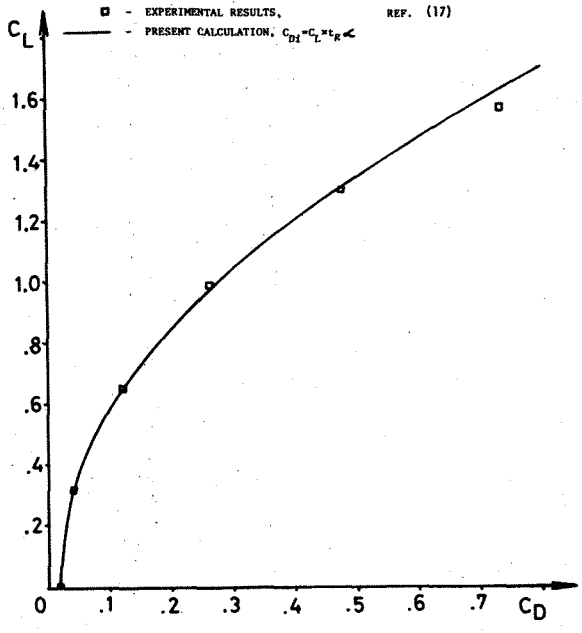


FIGURE 9 - LIFT COEFFICIENT Vs. DRAG COEFFICIENT, CONFIGURATION No. 2.

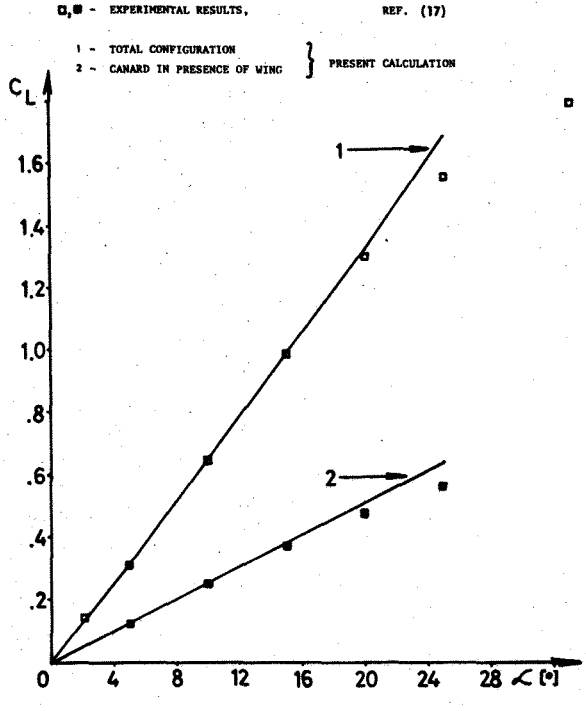


FIGURE 8 - LIFT COEFFICIENT Vs. ANGLE OF ATTACK, CONFIGURATION No. 2.

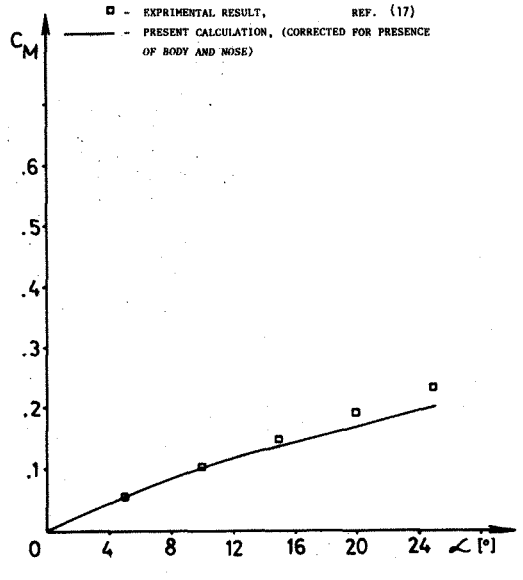


FIGURE 10 - PITCHING MOMENT COEFFICIENT Vs. ANGLE OF ATTACK, CONFIGURATION No. 2.

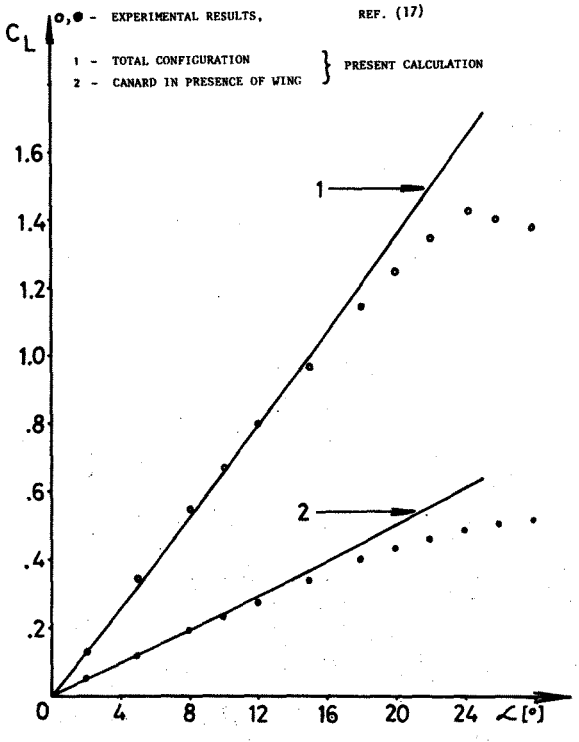


FIGURE 11 - LIFT COEFFICIENT Vs. ANGLE OF ATTACK, CONFIGURATION No. 3.

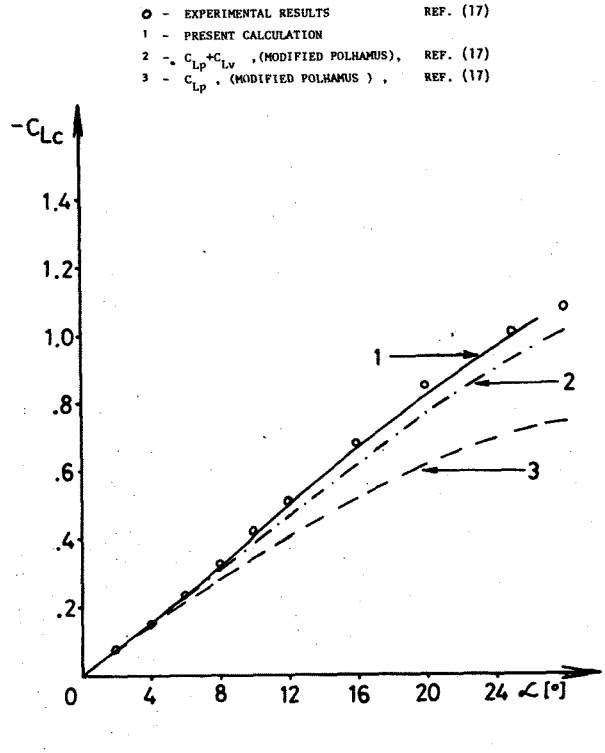


FIGURE 13 - COMPARISON OF EXPERIMENTAL RESULTS TO VARIOUS THEORETICAL RESULTS FOR CONFIGURATION No. 2.

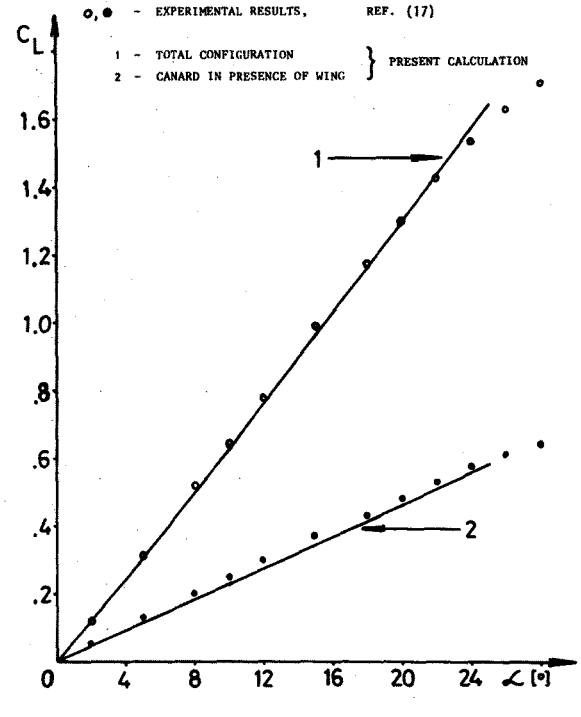


FIGURE 12 - LIFT COEFFICIENT Vs. ANGLE OF ATTACK, CONFIGURATION No. 4.

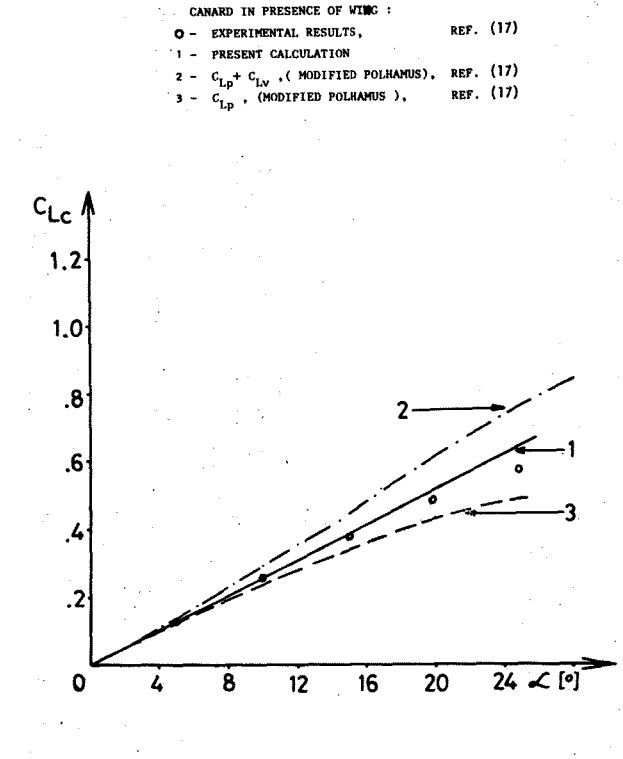


FIGURE 14 - COMPARISON OF EXPERIMENTAL RESULTS TO VARIOUS THEORETICAL RESULTS FOR CONFIGURATION No.2.

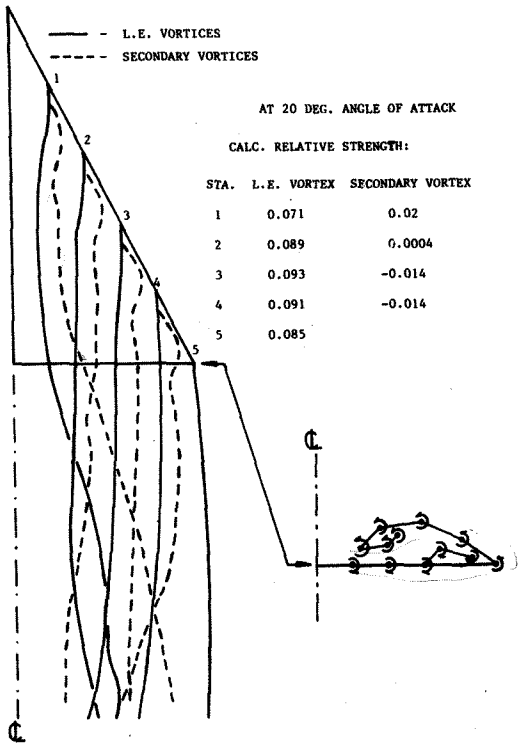


FIGURE 15 - LEADING EDGE VORTICES AND SECONDARY VORTICES CALCULATED FOR DELTA WING OF AR = 2.

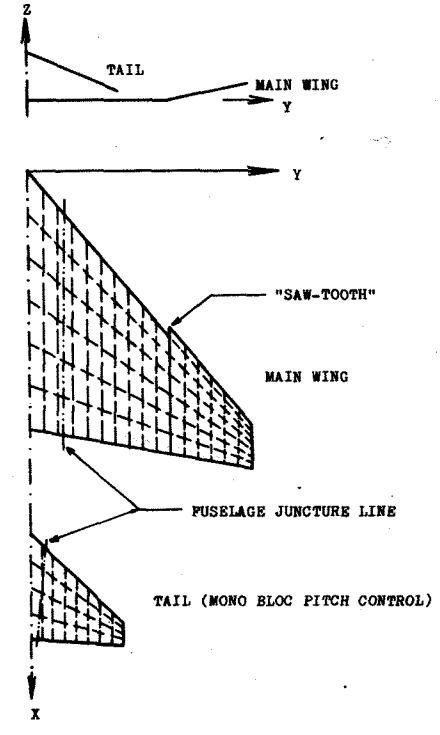


FIGURE 16 - SCHEMATIC DESCRIPTION OF THE MODEL OF AN F-4-E PARTITIONED INTO ELEMENTAL PANELS.

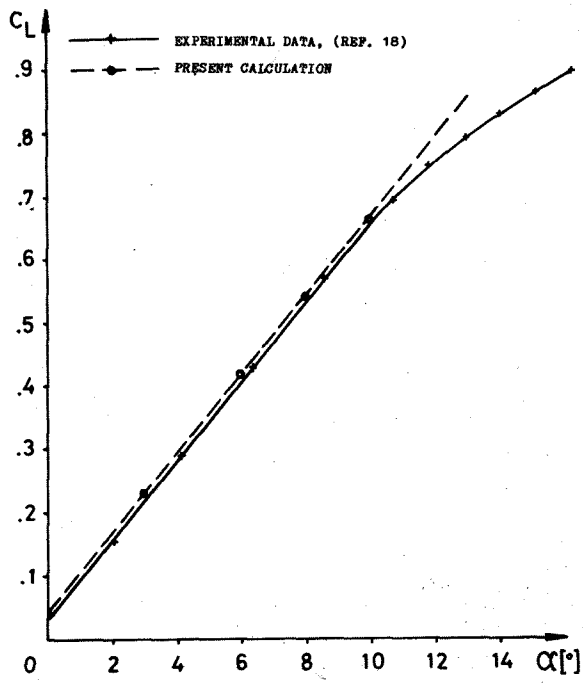


FIGURE 17 - LIFT COEFFICIENT Vs. ANGLE OF ATTACK, F-4-E MODEL, AT 0.6 MACH NUMBER.

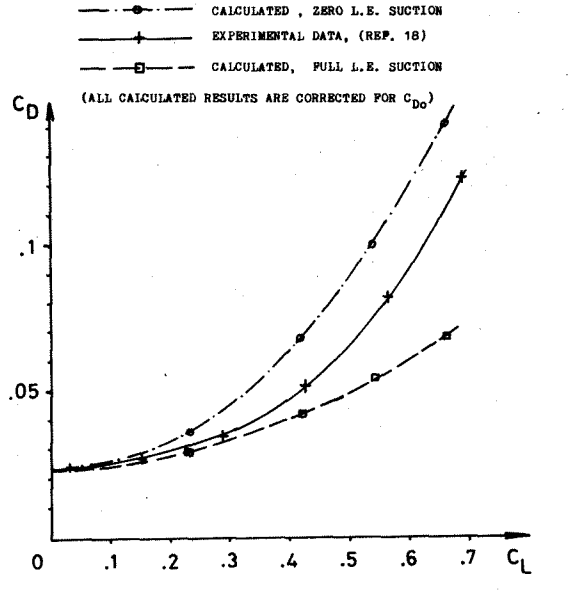


FIGURE 18 - TOTAL DRAG COEFFICIENT Vs. LIFT COEFFICIENT, F-4-E MODEL AT 0.6 MACH NUMBER.

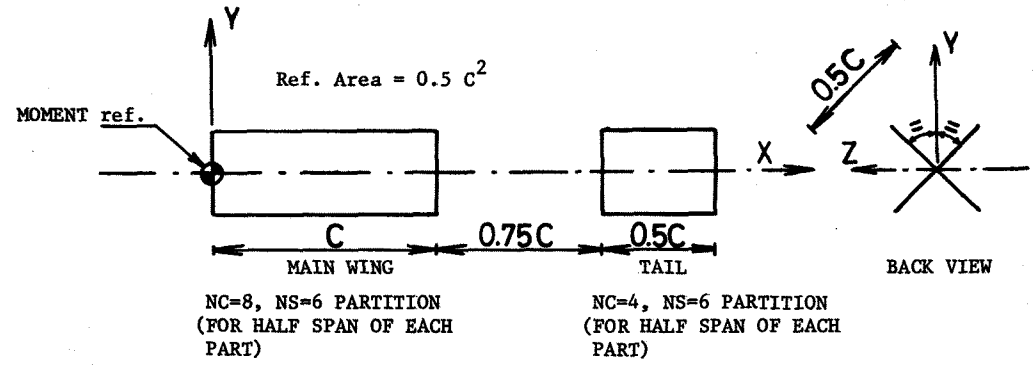


FIG. 19 - DESCRIPTION OF THE CRUCIFORM MODEL

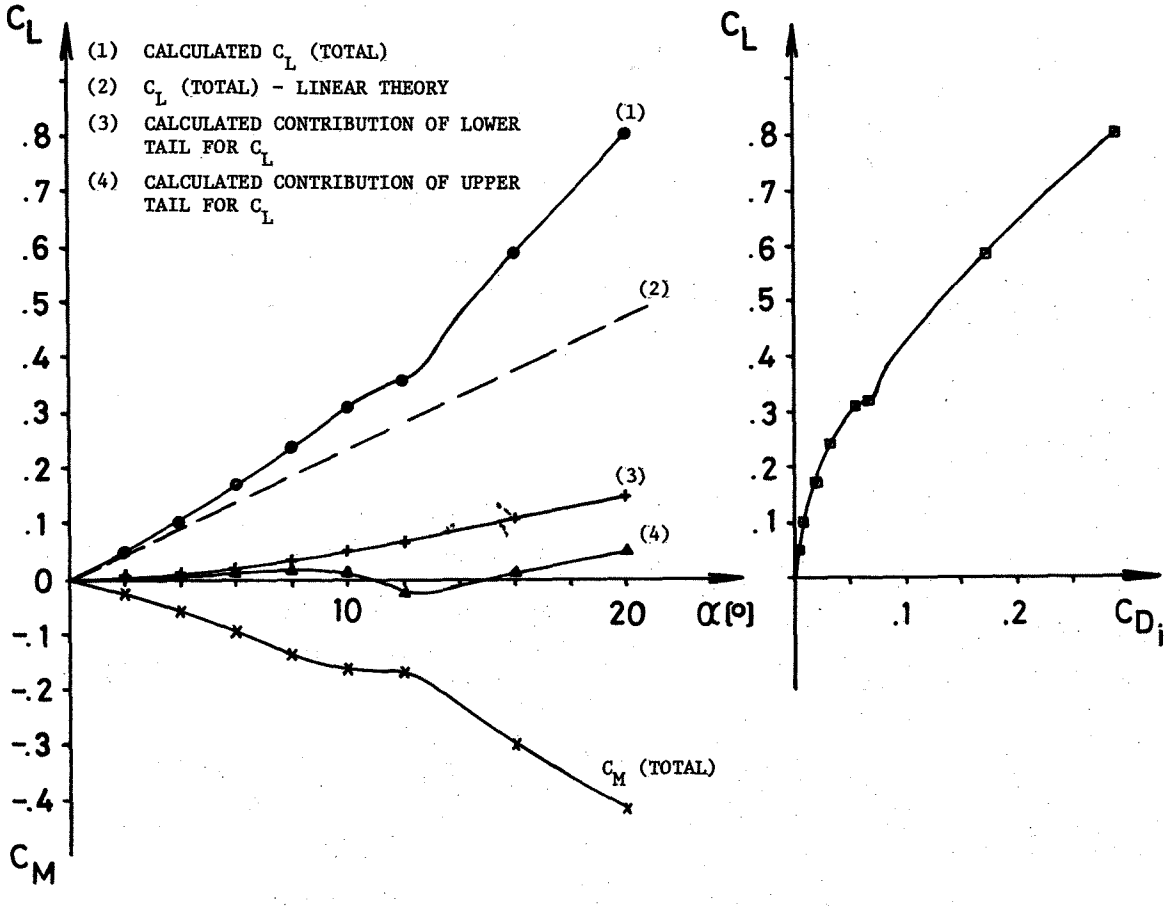


FIG. 20 - LIFT AND PITCHING MOMENT COEFFICIENTS Vs. ANGLE OF ATTACK; INDUCED DRAG COEFFICIENT Vs. LIFT COEFFICIENT, CALCULATED FOR THE CRUCIFORM CONFIGURATION